2019

Structural Engineering of Hierarchical Micro-nanostructured Ge-C Framework by Controlling the Nucleation for Ultralong Life Li Storage

Shilin Zhang
University of Wollongong, sz384@uowmail.edu.au

Yang Zheng
University of Wollongong, *Wuhan University of Science and Technology*

Xuejuan Huang
South-Central University for Nationalities, xjhuang@yahoo.cn

Jian Hong
University of Wollongong, jh590@uowmail.edu.au

Bin Cao
University of Wollongong, *Beijing University of Chemical Technology*

See next page for additional authors

Publication Details

Zhang, S., Zheng, Y., Huang, X., Hong, J., Cao, B., Hao, J., Fan, Q., Zhou, T. & Guo, Z. (2019). Structural Engineering of Hierarchical Micro-nanostructured Ge-C Framework by Controlling the Nucleation for Ultralong-Life Li Storage. Advanced Energy Materials, 9 (19), 1900081-1-1900081-11.

Structural Engineering of Hierarchical Micro-nanostructured Ge-C Framework by Controlling the Nucleation for Ultralong Life Li Storage

Abstract

The rational design of a proper electrode structure with high energy and power densities, long cycling lifespan, and low cost still remains a significant challenge for developing advanced energy storage systems. Germanium is a highly promising anode material for high-performance lithium ion batteries due to its large specific capacity and remarkable rate capability. Nevertheless, poor cycling stability and high price significantly limit its practical application. Herein, a facile and scalable structural engineering strategy is proposed by controlling the nucleation to fabricate a unique hierarchical micro-nanostructured Ge-C framework, featuring high tap density, reduced Ge content, superb structural stability, and a 3D conductive network. The constructed architecture has demonstrated outstanding reversible capacity of 1541.1 mA h g −1 after 3000 cycles at 1000 mA g −1 (with 99.6% capacity retention), markedly exceeding all the reported Ge-C electrodes regarding long cycling stability. Notably, the assembled full cell exhibits superior performance as well. The work paves the way to constructing novel metal-carbon materials with high performance and low cost for energy-related applications.

Keywords

controlling, nucleation, framework, ge-c, micro-nanostructured, hierarchical, engineering, structural, li, storage, ultralong-life

Disciplines

Engineering | Physical Sciences and Mathematics

Publication Details

Zhang, S., Zheng, Y., Huang, X., Hong, J., Cao, B., Hao, J., Fan, Q., Zhou, T. & Guo, Z. (2019). Structural Engineering of Hierarchical Micro-nanostructured Ge-C Framework by Controlling the Nucleation for Ultralong-Life Li Storage. Advanced Energy Materials, 9 (19), 1900081-1-1900081-11.

Authors

Shilin Zhang, Yang Zheng, Xuejuan Huang, Jian Hong, Bin Cao, Junnan Hao, Qining Fan, Tengfei Zhou, and Zaiping Guo

DOI:10.1002/201900081
Article paper: Full paper

Structural Engineering of Hierarchical Micro-nanostructured Ge-C Framework by Controlling the Nucleation for Ultralong-life Li Storage

Shilin Zhang[†], *Yang Zheng*[†], *Jian Hong*, *Bin Cao*, *Junnan Hao*, *Qining Fan*, *Tengfei Zhou*[*], *Zaiping Guo*[*]

S. Zhang, Dr. Y. Zheng, J. Hong, Dr. B. Cao, J. Hao, Q. Fan, Dr. T. Zhou, Prof. Z. Guo

Institute for Superconducting and Electronic Materials (ISEM), Australian Institute for Innovative Materials (AIIM), School of Mechanical, Materials, Mechatronics and Biomedical Engineering, University of Wollongong, Wollongong, 2522, Australia

Dr. Y. Zheng, Ms. X. Huang, Dr. T. Zhou,

College of Chemistry and Materials Science, South-Central University for Nationalities, Wuhan, 430074, P. R. China

Email:tengfeizhou2009@hotmail.com (T. Z), zguo@uow.edu.au (Z.P.G)

† These authors contributed equally to this work.

Keywords: structural engineering, micro-nanostructures, germanium-carbon frameworks, mechanism understanding, lithium storage

The rational design of a proper electrode structure with high energy and power densities, long cycling lifespan, and low cost, still remains a significant challenge for developing advanced energy storage systems. Germanium is a highly promising anode material for high-performance lithium ion batteries due to its large specific capacity and remarkable rate capability. Nevertheless, the poor cycling stability and high price significantly limit its practical application. Herein, we proposed a facile and scalable structural engineering strategy by controlling the nucleation to fabricate a unique hierarchical micro-nanostructured Ge-C framework, featuring high tap density, reduced Ge content, superb structural stability, and a three-dimensional conductive network. The constructed architecture demonstrated outstanding reversible capacity of 1541.1 mA h g^{-1} after 3000 cycles at 1000 mA g^{-1} (with 99. 6% capacity retention), markedly exceeding all the reported Ge-C electrodes regarding long cycling stability. Noticeably, the assembled full-cell exhibited superior performance as well. The work paves the way to constructing novel metal-carbon materials with high performance and low cost for energy-related applications.

1. Introduction

Germanium is an attractive electrode material for future high-energy lithium ion battery (LIBs, especially for batteries in sophisticated fields such as communications, deep-space exploration and national defence),[1] because of its high volumetric/gravimetric capacities (8645.9 mA h cm^{-3} and 1600 mA h g^{-1}, respectively),[2] favourable (de)lithiation voltage (< 0.5 V *vs.* Li/Li^+), excellent lithium-ion diffusivity (over 400 times faster than in Si),[3] and remarkable electrical conductivity (104 times higher than Si). Besides, unlike the highly anisotropic lithiation in Si, the isotropic lithiation behaviour in Ge anode ensures favorably reversible capacity.[4] Nevertheless, the practical applications of micro-sized bulk Ge have been hampered by some fundamental problems. First, the considerable volume change of 370% in the fully lithiated $Li_{4.4}Ge$ triggers severe electrode pulverization and solid-electrolyte interphase (SEI) film destabilization, resulting in rapid capacity fading as well as poor Coulombic efficiency (CE). Second, the low atomic utilization in the bulk phase of the microsized electrode will sacrifice some theoretical capacity of the Ge anode. Finally, simultaneously retaining the high performance but lowering the price of Ge anodes is still a critical challenge.

Over the past decade, considerable efforts have been devoted to improving the cycling performance of Ge anodes by designing various nanoarchitectures, such as nanoparticles, nanotubes, nanowires, and porous particles.[4-5] These constructed nanostructures could effectively relieve internal strain upon cycling and improve the utilization efficiency of Ge at the atomic level, thus achieving better electrochemical properties than their bulk counterparts. Despite some progress, such nanostructured design of Ge electrodes has also introduced tough new challenges, inevitably blocking the commercialization of nano-sized Ge in high-energy LIBs. Specifically, the intrinsic low tap density owing to the loose stacking will result in low volumetric energy density, while the large surface area may exacerbate side reactions and lower the coulombic efficiency.[6] Furthermore, the reduced electrical connections among

nanoparticles induced by volume changes could lead to unsatisfactory capacity retention.[3] Coating or encapsulating nanosized Ge with carbonaceous materials could further enhance the cycling properties of electrodes via suppressing the volume changes and alleviating nanoparticles agglomeration. For example, by encapsulating Ge nanoparticles in carbon nanotubes (CNTs), Loh et al developed novel bamboo-type multiwall CNTs as a matrix for the Ge particles and achieved high capacity and rate capability, due to the mechanical protection of the unique CNT scaffold structure.[7] A three-dimensional (3D) nanoarchitecture of Ge coated with carbon (3D-Ge/C) has been fabricated and exhibited outstanding cyclability and rate capacity.[8] Unfortunately, till now, most of the reported Ge-C composites are typically designed by randomly combined the nano-sized Ge with carbon materials and constructed the primary hybrid structure, which cannot adequately tackle all the above challenges. The long-term cycling stability for Ge-based anodes is still far from the practical application.[9] Moreover, the high cost derived from the relatively high ratio of Ge (generally over 60%) in those previously developed Ge-C nanocomposite electrodes makes them unattractive for large-scale utilization.

To completely utilize the promising high-capacity of Ge, rational design and controllable synthesis are highly desirable to develop novel Ge electrodes with a superior structure that can afford high energy density, improved power density, ultra-long lifetime, and low cost. Some fascinating structural designs, such as yolk-shell,[10] core-shell,[11] and pomegranate hierarchical assemblies [6a] have shown good effects in improving the cycle life of Si anodes towards inhibiting the severe pulverization and rapid deterioration of electrodes.[2] Such structures are beneficial to achieve good structural stability, generate a robust SEI layer, and minimize side reactions, consequently contributing to superior cyclability. Very recently, a novel 3D yolk-shell nanoarchitecture constructed by encapsulating Ge quantum dots with nitrogen-doped graphene foam and nitrogen-doped graphene outer shell shown excellent rate and cycling stability for Li storage.[12] However, the inferior volumetric density of nanomaterials as

mentioned above will restrict their real application. Also, the elaborate multi-step synthesis procedure for the Ge-C materials is complicated and energy-consuming, and thus not favourable for practical applications.

Herein, we developed a facile and scalable structural engineering strategy to fabricate a hierarchical micro-nanostructured Ge-C framework (GCF) by controlling the nucleation in a confined vacuum environment. In this unique design, single Ge nanoparticles (GeNPs) are conformably and individually encapsulated by an amorphous carbon layer and assembled into the secondary microstructure from the primary Ge-C hybrid nanostructures, while a continuous outer carbon layer then surrounds the assembly. This ingenious design endows the constructed Ge/C anode with some superior advantages: 1) high tap density ensured by the well-defined micro-nanostructure; 2) excellent structural stability and mechanical integrity benefited from the conformable nano-confinement effect; 3) fast charge transfer dynamics derived from the continuous 3D conductive network; 4) high coulombic efficiency due to the stabilized SEI films and reduced electrode–electrolyte contact area; and 5) a relatively low amount of Ge, reducing the total cost of the composite electrode to meet the practical requirements. As expected, the as-prepared hierarchical micro-nanostructured Ge-C framework obtained at 500°C (GCF-500) exhibited superior Li-ion storage performance, including ultra-high utilization of Ge (2078.8 mA h g^{-1} at 100 mA g^{-1}), excellent high-rate capability (1110.7 mA h g^{-1} at 20 A g^{-1}), and ultra-long cycling stability (> 3000 cycles, with 99. 62% capacity retention). Moreover, the assembled full cells demonstrated good performance as well, suggesting the great promise of the constructed GCF-500 anode for next-generation high-energy LIBs. The developed synthesis strategy and proposed evolution mechanism can be extended to the design and fabrication of other high-performance materials for energy storage or conversion systems.

2. Discussions and Results

2.1. Materials synthesis and characterisation of the Ge-carbon frameworks

The GCF sample with hierarchical micro-nanostructures was prepared from a commercially available tetraphenylgermanium (TPG) precursor by controlling its nucleation in a closed vacuum space. Noticeably, the vacuum environment is a crucial factor for the formation of the GCF samples. To fully understand the growth mechanism and evolution process, the TPG precursor was separately annealed under a sealed vacuum environment from 400 to 1050°C, respectively. The detailed discussion about the evolutionary mechanism can be seen in the supporting information. (Section S1 and Figure S1 to S3). The proposed three-step evolution process (including the "Interlinking and sublimation", "Decomposition and nucleation", and "Growth and aggregation") for the formation of GCF samples by pyrolysis of metallic phenyl compounds under space-confined vacuum environment is schematically illustrated in Figure 1A. More specifically, when TPG precursors were heated to both 400°C and 450°C, the solid powder would undergo a direct sublimation, instead of the melting progress, generating the spherical grains at 400°C. Furthermore, the derived vapour precursor can be decomposed to metallic Ge particles and amorphous carbon with hierarchical micro-nanostructure at 500 °C. The hierarchical structure could be maintained when the pyrolysis temperature was lower than 700°C. Finally, the micro-sized core-shell structure can be generated when treated at a higher temperature (800°C). Interestingly, due to the much higher pyrolysis temperature of 1050°C, the greatly graphitized carbon layer also grew on the outer surface of the core-shell structure. To highlight the advantage of the developed novel design concept for Ge/C anodes in this work, we systematically studied three representative Ge-C frameworks, namely the hierarchical micro-nanostructured Ge/C framework (GCF-500), the nano-Ge/C framework with core-shell structure (obtained at 800°C, GCF-800), and the micro-Ge/C framework with core-shell structure (obtained at 1050°C, GCF-1050).

The as-prepared GCF-500 sample presents a uniform spherical structure with an average diameter of about 2-3 μm, as clearly observed in the SEM images (Figure 1B, Figure S1F, and Figure S1G). More interestingly, excellent primary Ge nanoparticles (around 45 nm) are

conformably encapsulated and individually isolated by the interlinked carbon shell due to the in-situ decomposition and carbonization of the TPG molecules under space-confined vacuum condition (Figure 1E). The continuous carbon frameworks are predominantly generated from the gas species in the step that decomposed to oligomers, acetylene, radicals, and hydrogen at around 500°C, very similar to the derivatives from benzene-based materials after thermal treatment.[13] In addition, Figure 1H shows these primary GeNPs with the obvious (111) and (220) crystal planes. The corresponding interlayer distances were further determined to be around 0.327 nm and 0.200 nm, respectively (Figure 1I). The selected area electron diffraction (SAED) pattern (Figure 1J) also displays a set of diffraction rings from *cubic* Ge, corresponding to the diffractions of the (111), (220), (311), and (400) planes, respectively. The high-angle annular dark-field scanning TEM (HAADF-STEM) micrograph and energy dispersive X-ray spectroscopy (EDX) elemental mapping images both illustrate the presence of Ge, C, and O elements with homogeneous distributions in the GCF-500 material (Figure 1K), where the oxygen may come from the partial oxidization of surface Ge or absorbed air.[14]

As for other GCF samples that obtained at a further elevated temperature (above 500°C), their spherical structures are well preserved (Figure 1C and Figure 1D). However, a large amount of GeNPs tended to move inward in the carbon shell with randomly stacked and embedded morphology in GCF-800 (Figure S4). The uneven distributions of Ge particle sizes ranging from 30 to 500 nm indicate the accelerated nucleation and growth kinetics of GeNPs under higher reaction temperature, resulting in the severe aggregation of the GeNPs and the formation of core-shell structure (Figure 1F and Figure S4C). Similarly, EDX mapping of a typical spherical structure reveals the irregular distributions of Ge, C, and O elements (Figure S4E), in which the centre of the framework shows a higher concentration of Ge compared to the edge section. Importantly, when the processing temperature was increased to 1050 °C, the spontaneous aggregation process of GeNPs could be significantly boosted, leaving a microsized Ge particle inside of the carbon matrix, as clearly shown in Figure1G and Figure S5.

Furthermore, the appearance of multilayers with tens of nanometers length on the outer surface of the carbon shell can be easily observed from the SEM images in GCF-1050 (Figure S5B) and HRTEM images (Figure S5C and D). The HAADF-STEM images in Figure S5E show the corresponding elemental distributions of Ge, C, and O elements within those microsized spheres.

It is clearly shown that the described strategy is a facile and controllable method to fabricate various micro-sized Ge-C frameworks with fascinating structures, including the core-shell, micro-nano and the hierarchical structure by regulating the nucleation dynamics of the TPG molecules under different heated temperature. During the transformation process from the TPG precursor to the final Ge-C product, the space-confined system and the reaction temperature will significantly affect the nucleation pathways of TPG molecules on the nanoscale. From our understanding of the evolution mechanism of TPG, a continuous three-step process can be induced into a closed vacuumed system, unlike the direct sublimation without any decomposition process in the open inert system. Considering that, in a sealed vacuumed system, the critical step was demonstrated to be the nucleation of new species in the reaction resulting from the decomposition of TPG. The designed GCF-500 with the unique hierarchical arrangement and ultra-homogeneous distributions of GeNPs can be obtained under this kind of moderate reaction kinetics at the critical point (500°C) in which precursor will be decomposed and new species will be formed, contributing the isotropic growth of GeNPs in all directions.

The structures and the chemical states of GCF were further characterized. Figure 2A shows typical XRD patterns of GCF-500, GCF-800, and GCF-1050 samples. All the distinct diffraction peaks can be well indexed to *cubic* germanium (JCPDS #04-0545). With increasing reaction temperature from 500 to 1050°C, the decreased values of the full width at half-maximum (FWHM) further indicate the increasing crystal size of GeNPs from GCF-500 to GCF-1050. Although the reflections of carbon is dominantly influenced by intensive (111) facet of Ge, its existence and the defect level can be clearly confirmed by Raman spectroscopy (Figure S2B) and HRTEM images (Figure S6). As shown in Fig 2B, the intensity ratio (2.08)

of the defect (D) band to the graphitized (G) band of carbon (I_D/I_G) in GCF-500 is much higher than for GCF-800 (1.83) and GCF-1050 (1.45). The high ratio of disordered carbon with abundant defects formed in the GCF-500 would boost Li ions diffusion kinetics, thus enhancing the high-rate capability during electrochemical cycling in LIBs. [17] Additionally, the high graphitization of carbon layers with obvious fringes on the outer surfaces of GCF-1050 (Figure S6C) were derived from the catalytic decomposition of H and C atoms chemically adsorbed on the surface of Ge. [14, 18] Furthermore, XPS analysis of Ge 3d was performed here to investigate the surface electronic state and chemical environment of the Ge species (Figure 2C). Interestingly, the peaks of the Ge-Ge band shifted toward lower binding energy when compared to the commercial Ge samples, signifying the improved conductivity of metallic Ge in the GCF samples, which will be beneficial to promote the dynamics of electrons transfer during electrochemical reactions. This result is quite similar to the phenomenon in carbon nanotube where conductivity is improved by the *p-type* heteroatom doping effect.[19] The C 1s spectrum of GCF sample (Figure S6D) can be divided into four dominant peaks.[20] The one at around 284.6 eV corresponds to conjugated C=C/C-C bonds, while the peak at 285.9 eV, 287.0 eV, and 289.1 eV are due to the vibration of C-OH, C=O, and π- π* bonds, respectively. A relatively higher proportion of peaks at around 284.6 eV are observed in the GCF-800 and GCF-1050 samples, indicating a much higher degree of graphitization (Figure S6E and F). Moreover, to quantitatively evaluate the Ge content in the GCF materials, Thermogravimetric analysis (TGA) was conducted in the air environment. As illustrated in Figure 2D and Figure S7, the Ge contents in GCF-500, GCF-800, and GCF-1050 were determined to be about 40.1, 21.9, and 19.5 wt.%, respectively. This is mainly owing to the thorough decomposition of tiny molecular (oligomers and acetylene) derived from phenyl to carbon species under high temperatures during the thermal procedures. [13c] When considering the application of high-energy LIBs, particularly for miniaturized electrical devices (such as small drones, microsatellites, or national defence), [21] the volumetric energy density is a much more important indicator than gravimetric

energy density, and consequently, electrode materials with high tap density are highly needed. Here, the measured tap density of the GCF-500 is 0.97 g cm^{-3}, which is larger than that of the GCF-800 (0.76 g cm^{-3}) and GCF-1050 (0.71 g cm^{-3}), respectively (Figure 2E). Impressively, the achieved tap density of the GCF sample with hierarchical micronano-sized framework is visibly higher than those reported bulk Ge-C structures, [6b] hard carbon, [22] and oxidized pristine graphite materials.[23] Particularly, the hierarchically assembled and tightly packed GeNPs in the GCF-500 greatly enhanced the tap density of the sample, thus offering desired high volumetric energy density for LIBs. According to the results of structure characterization, it is reasonable to believe that, the designed hierarchical micro-nanostructured GCF-500 could be presented as a highly promising anode material toward high-energy LIBs, because of its following merits : i) the space-confined arrangement of Ge particles in the carbon shell can improve the utilization of those particles; ii) the interlinked carbon frameworks are able to serve as a buffer to effectively tolerate the huge volume expansion; iii) the improved conductivity of Ge and amorphous character of carbon could promote charge transport kinetics; and (iv) enhanced tap density will help to improve the volumetric density of the electrode.

2.2 Electrochemical performance of the as-designed GCF as anodes for LIBs

The electrochemical performance of the prepared GCF-500 was first investigated by cyclic voltammetry (CV) curves in a half-cell within the voltage window of 0.01–1.5 V (Figure 3A). In the initial cathodic scan, two peaks located at 1.31 and 0.7 V can be ascribed to the irreversible reactions of lithium and the formation of the SEI layers.[6b] In the second cathodic scan, there are several peaks detected in the range between 0.5 and 0.05 V, corresponding to the formation of different Li_xGe (from Li_9Ge_4 to $Li_{22}Ge_5$) alloys during the lithiation process,[5b, 24] while the prominent oxidation peaks at around 0.59 and 0.75 V can be assigned to the multistep de-alloying reactions of Li_xGe alloy. The GCF-800 and GCF-1050 samples both present CV behaviour with similar shapes to those in the GCF-500, but with slightly different voltage values and inferior reversibility during the scans (Figure S8). Furthermore, Figure 3B

shows the initial galvanostatic charge-discharge voltage profiles of the GCF-500 electrode at a current density of 100 mA g^{-1}. In the first cycle, the GCF-500 exhibits discharge and charge capacities of 1263.6 and 895.9 mA h g^{-1}, respectively, which corresponds to an initial Coulombic efficiency (ICE) of 70.9 %. In contrast, the GCF-800 and GCF-1050 electrodes show a lower first-cycle reversible capacity of 696.6 and 521.6 mA h g^{-1}, corresponding to an ICE of 66.7% and 59.6%, respectively (Figure S9). This could be attributed to the high atomic Ge utilization ratio (Table S1), maintaining the integral stability of its whole structure caused by intimate attachment of GeNPs to outer carbon shell, as well as stable SEI layers formed on the outer surface of GCF-500. Moreover, after 50 continuous cycles at 100 mA g^{-1}, the capacity of GCF-500 electrode was still stabilized at around 833.6 mA h g^{-1} (Figure 3C, corresponding to 2078.8 mA h g^{-1} based on Ge), demonstrating the superior structural stability of GeNPs conformably and individually confined by the amorphous carbon layer in the GCF-500 sample.

The rate capabilities under various current densities were systematically studied for the GCF materials. As shown in Figure 3D, the GCF-500 maintained impressed reversible capacities of 880.4, 815.6, 771.5, 740.4, 702.8, 668.0, 632.0, and 566.9 mA h g^{-1}, at the current densities of 0.1, 0.2, 0.3, 0.5, 1, 2, 5, and 10 A g^{-1}, respectively. The capacity remained as high as 445.4 mA h g^{-1} (based on Ge: 1110.7 mA h g^{-1}) even when the current density increased to 20 A g^{-1} (about 3 min for complete charging and discharging process). While GCF-800 maintained only 102.4 mA h g^{-1} (based on Ge: 467.6 mA h g^{-1}) and GCF-1050 maintained about 212.1 mA h g^{-1} (based on Ge: 1087.7 mA h g^{-1}). When the current density was reduced back to 0.1 A g^{-1}, the reversible capacity of GCF-500 was restored to as high as 770.4 mA h g^{-1}, which is significantly higher than for its GCF-800, GCF1050, commercial Ge, and commercial GeO_2 counterparts (Figure S10 and Figure S11).

To further evaluate the long-term cycling performance, the electrodes were then charged/discharged at 1000 mA g^{-1} with prolonged cycling. As depicted in Figure 3E, the GCF-500 delivers a much more stable ultralong cycling performance. Even after 3000 cycles, over

618.3 mA h g^{-1} could be retained for the GCF-500 (corresponding to 1541.1 mA h g^{-1} based on Ge), demonstrating its excellent long-term cycling stability. More importantly, considering the 1600 mA h g^{-1} theoretical capacity of Ge, the electrochemical utilization of Ge atoms of GCF-500 is as high as 96.3% at a rate of 1000 mA g^{-1} for over 3000 cycles, which is the highest capacity and best Ge utilization ratio reported till now. From the 10^{th} to the 3000^{th} cycle, the coulombic efficiencies stabilized at above 99% with the lowest capacity fading-rate at 0.004% when compared to its counterparts: GCF-800, GCF-1050, commercial Ge, and commercial GeO_2. The specific comparisons and calculated values on voltage profiles and retentions of commercial graphite, Ge, and GeO_2 under identical current density are also summarized in Figure S12 to Figure S14. To the best of our knowledge, this is the first report of Ge-C anode material with such low capacity decay rate over 3000 cycles (detailed comparisons are presented in Figure S15, and Table S2 and S3), signifying the superb structural stability and mechanical integrity of the fabricated GCF-500 electrode during thousands of cycles.

The outstanding Li ions storage properties, such as the high reversible capacity, superior high-rate capability, and excellent long-term cyclability should be ascribed to the unique hierarchical micro-nanostructure of the designed GCF-500 material. Firstly, the homogeneously distributed and intimately contacted uniform fine of primary GeNPs with conductive carbon layer and constructed the secondary Ge-C hybrid nanoparticles in the hierarchical micro-sized Ge-C framework can maximize the utilization of Ge atoms during Li ions storage. Secondly, the continuous 3D carbon networks not only effectively tolerate the volume expansion of GeNPs and retain the structural integrity of the electrode during the repeated cycling, but also enhance the charge transfer processes. Thirdly, the formed robust SEI layer on the outer surface of micro-sized amorphous carbon networks can reduce the electrode–electrolyte contact area and consequently leading to high Coulombic efficiency. The SEM images of electrode structures after cycling test further confirmed the superior structural stability of the GCF-500 sample. After 200 deep charge/discharge cycles, the morphology of

the GCF with distinctive SEI formation was examined as shown in Figure 3 F to H. Impressively, the hierarchical micro-nanostructure in the GCF-500 electrode were well reserved with uniform and thin SEI layer coating on the outer surface of carbon networks, demonstrating the formation of robust SEI upon long cycling. In contrast, the GCF-800 and GCF-1050 electrodes suffered from severe carbon shell crack and pulverization (Figure 3 G and H). More severe problems of mechanical cracks can be observed in the electrodes of bare Ge nanoparticles and GeO_2 nanoparticles as well, due to the huge volume expansion of unprotected Ge (Figure S16). The cracking and pulverization of electrode frequently lead to rapid capacity decay and inferior cycle life of LIBs.[25] Hence, the robust SEI formed in the GCF-500 can contribute to high Coulombic efficiency and superior cyclability during long-term cycling.

To deeply understand the correlation between its structural advantages and the excellent electrochemical properties of GCF-500 electrode for LIBs, galvanostatic intermittent titration technique (GITT) measurements and electrochemical impedance spectroscopy (EIS) have been conducted, as shown in Figure 4. During GITT measurements, a constant current density was adopted for 0.5 h to obtain the closed-circuit voltage (CCV), and a 5 h pulse was applied to collect the quasi-open-circuit voltage (QOCV). The whole process can be regarded as a quasi-static process, and the reaction resistance can thus be obtained as well (Figure S17). Figure 4A presents the voltage responses of the GCF-500, GCF-800, and GCF-1050 electrodes in the third cycle. The ionic diffusion coefficient in GCF electrodes can be further determined by solving Fick's second law [26] with the specific equations presented in Materials and Methods. As indicated in Figure 4B and Figure 4D, the diffusion coefficients of hierarchical micro-nanostructured GCF-500 is nearly one order of magnitude higher than those of GCF-800 and GCF-1050 in both Li insertion and extraction processes during cycling. The larger diffusion coefficients in the GCF-500 electrode can be beneficial for enhancing the high-rate performance.[27] As presented in Figure 4C and 4E, the GCF-500 shows the lowest resistance

values compared to the other two GCF materials, indicating the boosted charge transfer dynamics and thus improving the high-rate performance of the electrode during lithiation/delithiation process. Similarly, the EIS diagram in Figure 4F shows that the GCF-500 has the lowest resistance among these three GCF electrodes (Figure S18), further confirming the increased electrode kinetics for Li ions storage. Taking into consideration the excellent electrochemical performance of GCF-500 anode (Figure 4G), in terms of its excellent high-rate capability, long-term durability, and ultra-high utilization ratio with relative low Ge content, it could be a promising anode material, which meets the practical requirements for most applications, such as military communications and deep-space exploration. [1] An additional advantage of our GCF is the synthesis does not involve any sophisticated equipment or processes such as chemical vapour deposition, showing a feasible and scalable way to design stabilized anodes for high-energy LIBs.

We have already demonstrated the elaborate synthesis of hierarchical micro-nanostructured GCF-500 and its structural benefits, kinetics advantages, and physical merits as a promising anode evaluated in a half-cell system. In addition, the practical application of GCF-500 as an anode in LIB was further evaluated by a full coin-cell constructed with a $LiFePO_4$ (LFP) cathode, as shown in Figure 5. A pre-lithiation procedure for GCF-500 was conducted to compensate the loss of lithium during the initial cycle with identical test conditions to those for the half-cell. The LFP was chosen as cathode owing to its highly stable capacity output and promising voltage platform (Figure S19). The charge-discharge voltage profiles for the 1^{st}, 2^{nd}, and 3^{rd} cycles are shown in Figure 5A. The primary discharge voltage platform for the full battery is around 2.8 V, which is very consistent with the potential gap between the discharge plateau of LFP (about 3.3 V) and that of GCF-500 (about 0.5V). After a continuous 50 cycles at 100 mA g^{-1}, the capacity of the full cell can also be stabilized at 634.6 mA h g^{-1} (Figure S20). Even after 500 cycles under the high current density value of 2000 mA g^{-1}, the full cell still delivers a capacity of 341.2 (based on Ge: 850.9 mA h g^{-1}) without apparent capacity fading in

the range of 1.5-3.7 V (Figure 5B). The 0.02 % decay per cycle further illustrates the excellent cycling stability of the coin-cell configuration based on the promising GCF-500 anode and LFP cathode. Compared the GCF-500 electrode with previously reported state-of-the-art Ge/C electrodes (Figure 5D), our hierarchical micro-nanostructured GCFs electrode could deliver the highest reversible capacity with ultralong cycling stability among all the anode materials.

3. Conclusion

Our designed strategy for constructing the germanium-carbon frameworks with attractive micro-nanostructures presented in this work is controllable, scalable and easily reproducible. The straightforward thermal treatment protocol of metal-organic compounds could be extended for the fabrication of an extensive series of other metal-carbon framework with tunable micro-nanostructures and high performance. Based on our obtained results, the sealed system design plays a crucial role in wisely governing the nucleation pathways on the nanoscale. The metal particle size, carbon graphitization, metallic conductivity, as well as morphology of GCFs can be regulated by flexibly controlling the reaction temperature to meet our different requirements on energy storage and conversion applications. From our understanding of the mechanism for the thermal behaviour, a continuous three-stage mode can be induced into this closed vacuumed system, which the critical step was demonstrated to be the nucleation of new species in the reaction resulting from the decomposition of TPG.

In our case, the smart design of the hierarchical micro-nanostructured Ge-carbon framework could allow it to effectively inherit the advantages of both microsized and nanosized structures thus fully tackling most of the issues involved in Ge-anodes. Specifically, the unique design possesses multiple structural advantages: *1.* the primary Ge nanoparticles can maximize the utilization of Ge atomics and relieve the induced internal strain during cycling; *2.* the closely packed secondary Ge-C hybrid nanoparticles could improve the tap density and prevent the aggregation of Ge nanoparticles; *3.* the conformable and isolated encapsulation of carbon layer will accommodate the huge volume exchange of Ge and offer high electrical conductivity; *4.* the microsized interconnected carbon shell completely covered the entire Ge-C hybrid nanoparticles could stabilize the SEI film and improve the columbic efficiency of the electrode.

In summary, a multi-functional hierarchical micro-nanostructured germanium-carbon framework (GCF-500) has been successfully synthesized by a facile and controllable nucleation-regulating strategy. Benefiting from its unique structural features, the constructed

GCF-500 electrode exhibited remarkable Li-ion storage properties, such as fast rate capability, high reversible capacity, and ultra-long cyclability. Notably, the achieved ultra-long cycling stability significantly surpass that of other Ge-C anodes. More impressively, the configuration of the full cell with GCF-500 anode and LFP cathode also exhibited superior electrochemical performance under higher current density. From a practical application point of view, the acceptable amount usage of Ge metal with ultra-high utilization ratio (96.3%), superior cyclability of Ge (3000 cycles), and stabilized capacity output for successful operation are primary requirements to allow high energy/power densities of Li-ion batteries. In this regard, it is believed that the hierarchical micro-nano structures reported here might re-establish Ge as promising anode materials for high-energy lithium-ion batteries.

4. Experimental Section

4.1. Synthesis of germanium-carbon frameworks:

An appropriate amount of commercially available metal-organic complex-tetraphenylgermanium (TPG) powder (96%, Alfa-Aesar) was first encapsulated in an evacuated quartz tube with the parameters of φ1.5 × 15 cm under ambient temperature. In the subsequent process, a furnace was heated to 500 °C at a ramping rate of 2 °C min^{-1} and kept at each target temperature for 4 hours to guarantee the complete reaction of TPG molecules in the tube. The uniform black germanium-carbon frameworks were deposited on the inner surface wall of the quartz tube. The frameworks could be readily peeled off after being soaked in ethanol under ultrasound. Under these conditions, the nanosized GCF-800 and microsized GCF-1050 samples were obtained at different pyrolysis temperatures of 800 °C and 1050 °C after holding at 500 °C for a duration of 4 hours, respectively.

4.2. Materials characterization:

The morphologies of the as-prepared products and after-cycling were observed by field emission scanning electron microscopy (FESEM, JEOL JSM-7500FA) operated at 15 kV and 20 mA. The details of the crystal structure were further examined by scanning transmission electron microscope (STEM, JEOL JEM-ARM200F), which was conducted at 200 kV, along with EDX mapping. The crystalline structure of the obtained materials was checked by X-ray diffraction (XRD, GBC MMA diffractometer) with Cu Kα radiation at a scanning rate of 1° min^{-1}. X-ray photoelectron spectroscopy (XPS) was investigated on a VG Multilab 2000 (VG Inc.) photoelectron spectrometer using monochromatic Al Kα radiation under vacuum at 2 × 10^{-6} Pa. All of the binding energies were referenced to the C 1s peak at 284.8 eV of the surface adventitious carbon. Raman analysis was performed with a JobinYvon HR800 Raman spectrometer. Thermogravimetric (TG) analysis was conducted on a Mettler Toledo TGA/DSC1 analyzer from 50 to 1000 °C in the air (20 sccm) with a ramp rate of 5 °C/min.

Assuming complete combustion of the carbon framework and conversion from Ge to GeO_2, the content of Ge in the GCF materials could be determined based on the equation in Figure S7.

4.3. Electrochemical Tests:

The electrochemical tests were conducted using CR 2032 coin-type cells. The working electrodes were prepared by mixing the obtained materials, Super P, and poly (acrylic acid) (PAA) in a weight ratio of 80:10:10. The resultant slurry was pasted on Cu foil and dried at 80 °C for 12 h in a vacuum, followed by pressing at 300 kg/cm^2. The weight of the materials on individual electrodes was about 0.9–1.1 mg cm^{-2}. Electrochemical measurements were carried out using two electrode coin cells with Li metal as a counter and a reference electrode and Celgard (product 2400) film as the separator. The electrolyte consisted of a solution of 1 M $LiPF_6$ in ethylene carbonate/dimethyl carbonate/ethyl methyl carbonate (1:1:1; v/v/v) with 5 wt. % fluoroethylene carbonate. Electrochemical impedance spectroscopy and cyclic voltammetry were conducted on a VMP-3 electrochemical workstation at a scan rate of 0.1 mV s^{-1}. GITT tests were also conducted on an Arbin SCTS battery tester at ambient temperature in the voltage range of 0.01–1.5 V. The cells were galvanostatically charged/discharged in the voltage range of 0.01–1.5 V versus Li/Li$^+$ at different current densities on a Land CT2001A battery tester, and the specific capacities were calculated based on the mass of the GCF if not mentioned, while for full cell $LiFPO_4$//GCF500 batteries, the voltage ranged from 1.5 to 3.7 V. In addition, to ensure the material utilization and reasonably evaluate the electrochemical performance of GCF-500, full-cells were assembled based on the capacity ratio of about 1:1.2 between the GCF-500 anode and LFP cathode, and the cell capacity was calculated based on the weight of the anode material only in this work. The weight of the materials for the full-cell test on individual electrodes was about 0.6-0.8 mg cm^{-2}. The Nyquist plots were obtained from over the frequency range of 100 kHz to 1 Hz.

Based on the GITT tests, the ionic diffusion coefficient (D_{Li+}) in the GCF electrodes can be determined by solving Fick's second law with the following Equation (1) based on the GITT curves, where m_a is the electrode active mass; M_a is the molar mass of the electrode material; V_M is the molar volume of electrode; S is the geometric area of the electrode; M_a/V_M is obtained from the density of the GCF electrode; and L is the average thickness of the electrode. A detailed definition of the parameters in the equation, including E_0, E_S, τ, t_0, $t_{0+\tau}$, E_τ, ΔE_S, and ΔE_τ in the GITT potential profiles is shown in Figure S16a.

$$D = \frac{4}{\pi\tau}\left(\frac{m_a V_M}{M_a S}\right)^2 \left(\frac{\Delta E_S}{\tau \times \frac{dE_\tau}{d\sqrt{\tau}}}\right)^2 \quad (\tau \ll L^2/D) \quad (1)$$

If the coin cell voltage is linearly proportional to $\tau^{1/2}$ (Figure S16b), Equation (1) can be further simplified to the following Equation (2):

$$D = \frac{4}{\pi\tau}\left(\frac{m_B V_M}{M_B S}\right)^2 \left(\frac{\Delta E_S}{\Delta E_\tau}\right)^2 \quad (2)$$

Supporting Information

Supporting Information is available from the Wiley Online Library or from the author.

Acknowledgments

Funding: Financial support provided by the Australian Research Council (ARC) (FT150100109, DP170102406, and DE190100504), the National Natural Science Foundation of China (51802357) and the Hubei Provincial Natural Science Foundation of China (2018CFB237) is gratefully acknowledged. **Author contributions: S.L.Z.** and **Y.Z.** contributed equally to this work. All the authors discussed the results and commented on the manuscript. The authors thank the Electron Microscopy Centre (EMC) at the University of Wollongong. The authors also thank Mr. Zhijie Wang and Ms. Sailin Liu for their help with

TGA tests and Dr. T. Silver for critical reading of the manuscript. **Competing interests**: The authors declare that they have no competing interests.

Received: ((will be filled in by the editorial staff))
Revised: ((will be filled in by the editorial staff))
Published online: ((will be filled in by the editorial staff))

References

[1] W. Chen, Y. Jin, J. Zhao, N. Liu, Y. Cui, *Proc. Natl. Acad. Sci.* **2018**, 201809344.

[2] W. Li, X. Sun, Y. Yu, *Small Methods* **2017**, 1, 1600037.

[3] D. S. Jung, M.-H. Ryou, Y. J. Sung, S. B. Park, J. W. Choi, *Proc. Natl. Acad. Sci.* **2013**, 110, 12229.

[4] S. Choi, J. Kim, N.-S. Choi, M. G. Kim, S. Park, *ACS Nano* **2015**, 9, 2203.

[5] a) M. H. Park, Y. Cho, K. Kim, J. Kim, M. Liu, J. Cho, *Angew. Chem. Int. Ed.* **2011**, 50, 9647; b) M.-H. Seo, M. Park, K. T. Lee, K. Kim, J. Kim, J. Cho, *Energy Environ. Sci.* **2011**, 4, 425.

[6] a) N. Liu, Z. Lu, J. Zhao, M. T. McDowell, H.-W. Lee, W. Zhao, Y. Cui, *Nat. Nanotechnol.* **2014**, 9, 187; b) D. Li, H. Wang, H. K. Liu, Z. Guo, *Adv. Energy Mater.* **2016**, 6, 1501666.

[7] W. Tang, Y. Liu, C. Peng, M. Y. Hu, X. Deng, M. Lin, J. Z. Hu, K. P. Loh, *J. Am. Chem. Soc.* **2015**, 137, 2600.

[8] D. T. Ngo, H. T. Le, C. Kim, J.-Y. Lee, J. G. Fisher, I.-D. Kim, C.-J. Park, *Energy Environ. Sci.* **2015**, 8, 3577.

[9] S. Wu, C. Han, J. Iocozzia, M. Lu, R. Ge, R. Xu, Z. Lin, *Angew. Chem. Int. Ed.* **2016**, 55, 7898.

[10] N. Liu, H. Wu, M. T. McDowell, Y. Yao, C. Wang, Y. Cui, *Nano Lett.* **2012**, 12, 3315.

[11] a) S. W. Lee, M. T. McDowell, L. A. Berla, W. D. Nix, Y. Cui, *Proc. Natl. Acad. Sci.* **2012**, 109, 4080; b) G. Jeong, J.-G. Kim, M.-S. Park, M. Seo, S. M. Hwang, Y.-U. Kim, Y.-J. Kim, J. H. Kim, S. X. Dou, *ACS Nano* **2014**, 8, 2977.

[12] R. Mo, D. Rooney, K. Sun, H. Y. Yang, *Nat. Commun.* **2017**, 8, 13949.

[13] a) K. C. Hou, H. B. Palmer, *J. Phys. Chem.* **1965**, 69, 863; b) K. Johansson, M. Head-Gordon, P. Schrader, K. Wilson, H. Michelsen, *Science* **2018**, 361, 997; c) D. Kostrin, M. Pikus, S. Trifonov, A. Lisenkov, presented at Journal of Physics: Conference Series **2017**.

[14] H. Kim, Y. Son, C. Park, J. Cho, H. C. Choi, *Angew. Chem.* **2013**, 125, 6113.

[15] a) J. Liang, R. F. Zhou, X. M. Chen, Y. H. Tang, S. Z. Qiao, *Adv. Mater.* **2014**, 26, 6074; b) E. Yoo, J. Nakamura, H. Zhou, *Energy Environ. Sci.* **2012**, 5, 6928; c) H. B. Wu, B. Y. Xia, L. Yu, X.-Y. Yu, X. W. D. Lou, *Nat. Commun.* **2015**, 6, 6512.

[16] Y. Zheng, T. Zhou, X. Zhao, W. K. Pang, H. Gao, S. Li, Z. Zhou, H. Liu, Z. Guo, *Advanced Materials* **2017**, 29, 1700396.

[17] a) Y. Li, L. Mu, Y.-S. Hu, H. Li, L. Chen, X. Huang, *Energy Storage Mater.* **2016**, 2, 139; b) T. Xia, W. Zhang, Z. Wang, Y. Zhang, X. Song, J. Murowchick, V. Battaglia, G. Liu, X. Chen, *Nano Energy* **2014**, 6, 109; c) A. D. Roberts, X. Li, H. Zhang, *Chem. Soc. Rev.* **2014**, 43, 4341.

[18] J.-H. Lee, E. K. Lee, W.-J. Joo, Y. Jang, B.-S. Kim, J. Y. Lim, S.-H. Choi, S. J. Ahn, J. R. Ahn, M.-H. Park, *Science* **2014**, 344, 286.

[19] a) H.-Z. Geng, K. K. Kim, K. P. So, Y. S. Lee, Y. Chang, Y. H. Lee, *J. Am. Chem. Soc.* **2007**, 129, 7758; b) W. Chen, S. Chen, D. C. Qi, X. Y. Gao, A. T. S. Wee, *J. Am. Chem. Soc.* **2007**, 129, 10418; c) R. Graupner, J. Abraham, A. Vencelová, T. Seyller, F. Hennrich, M. M. Kappes, A. Hirsch, L. Ley, *Phys. Chem. Chem. Phys.* **2003**, 5, 5472.

[20] J. Zhang, L. Qu, G. Shi, J. Liu, J. Chen, L. Dai, *Angew. Chem. Int. Ed.* **2016**, 55, 2230.

[21] a) J. W. Choi, D. Aurbach, *Nat. Rev. Mater.* **2016**, 1, 16013; b) A. Y. Song, Y. Xiao, K. Turcheniuk, P. Upadhya, A. Ramanujapuram, J. Benson, A. Magasinski, M. Olguin, L. Meda, O. Borodin, *Adv. Energy Mater.* **2018**, 8, 1700971; c) M. Li, J. Lu, Z. Chen, K. Amine, *Adv. Mater.* **2018**, 1800561.

[22] W. Xing, J. Xue, J. Dahn, *J. Electrochem. Soc.* **1996**, 143, 3046.

[23] Y. Wen, K. He, Y. Zhu, F. Han, Y. Xu, I. Matsuda, Y. Ishii, J. Cumings, C. Wang, *Nat. Commun.* **2014**, 5, 4033.

[24] K. H. Seng, M.-H. Park, Z. P. Guo, H. K. Liu, J. Cho, *Angew. Chem. Int. Ed.* **2012**, 51, 5657.

[25] H. Wu, G. Chan, J. W. Choi, I. Ryu, Y. Yao, M. T. McDowell, S. W. Lee, A. Jackson, Y. Yang, L. Hu, Y. Cui, *Nat. Nanotechnol.* **2012**, 7, 310.

[26] Y. You, H. R. Yao, S. Xin, Y. X. Yin, T. T. Zuo, C. P. Yang, Y. G. Guo, Y. Cui, L. J. Wan, J. B. Goodenough, *Adv. Mater.* **2016**, 28, 7243.

[27] Z. Li, J. Zhang, Y. Lu, X. W. D. Lou, *Sci. Adv.* **2018**, 4, eaat1687.

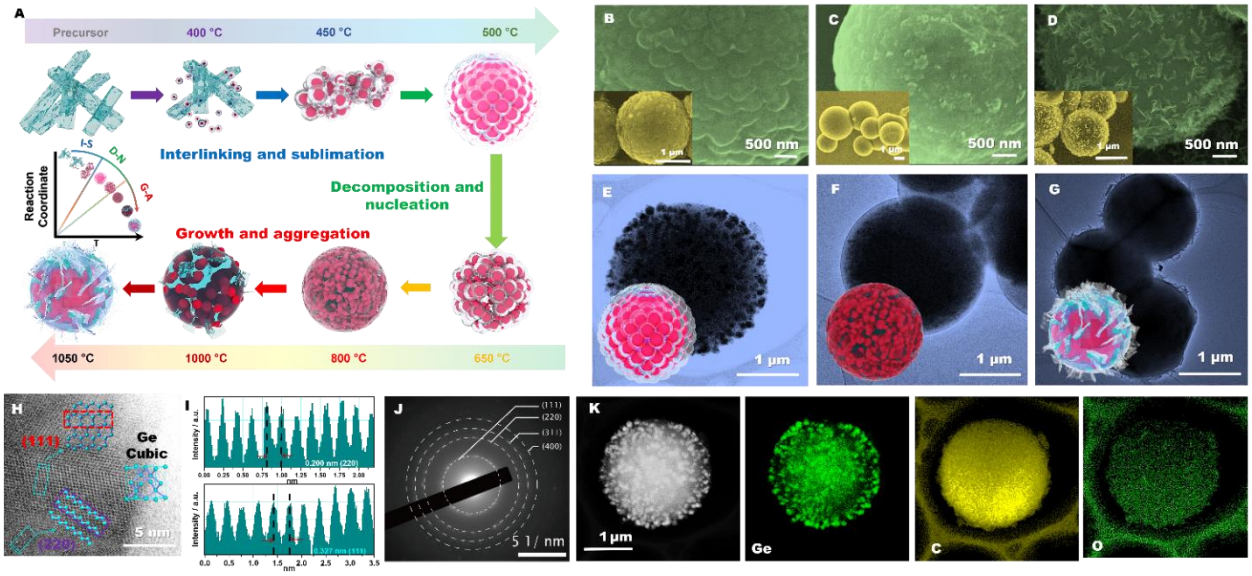

Figure 1 Schematic illustration, morphology, and structural characterization of Ge-carbon F materials. (A) Proposed growth mechanism of GCF samples through a facile confinement effect in evacuated tubes. In our sealed vacuum system, the distributions of GeNPs and carbon structures can be successfully controlled to form typical Ge-carbon frameworks (where the red dots indicate GeNPs from 500 to 1050 °C and the outer layer corresponds to the carbon shell). **SEM images** of **(insets:** lower magnifications**)**: **(B)** hierarchical micro-nanostructured GCF-500, **(D)** nano-Ge/C framework (GCF-800), and **(F)** micro-Ge/C framework (GCF-1050). **TEM images** of: **(C)** GCF-500, **(E)** GCF-800, and **(G)** GCF-1050. **(H)** HRTEM image of an individual Ge nanoparticle from GCF-500 (where the arrows indicate the facet parameters of (111) and (220); and the right bottom image shows the individual unit cell of *cubic* Ge crystal). **(I)** Intensity profiles of Ge crystal faces, the value of 0.327 nm relates to the (111) facet, and the value of 0.200 nm refers to the (220) facet of Ge, respectively. **(J)** The corresponding SAED pattern of a Ge particle in GCF-500. **(K)** HAADF-STEM image of individual GCF-500 sphere and its corresponding elemental mapping images of Ge, C, and O elements, respectively, which indicates the homogeneous distribution of Ge particles and a fully covered carbon shell.

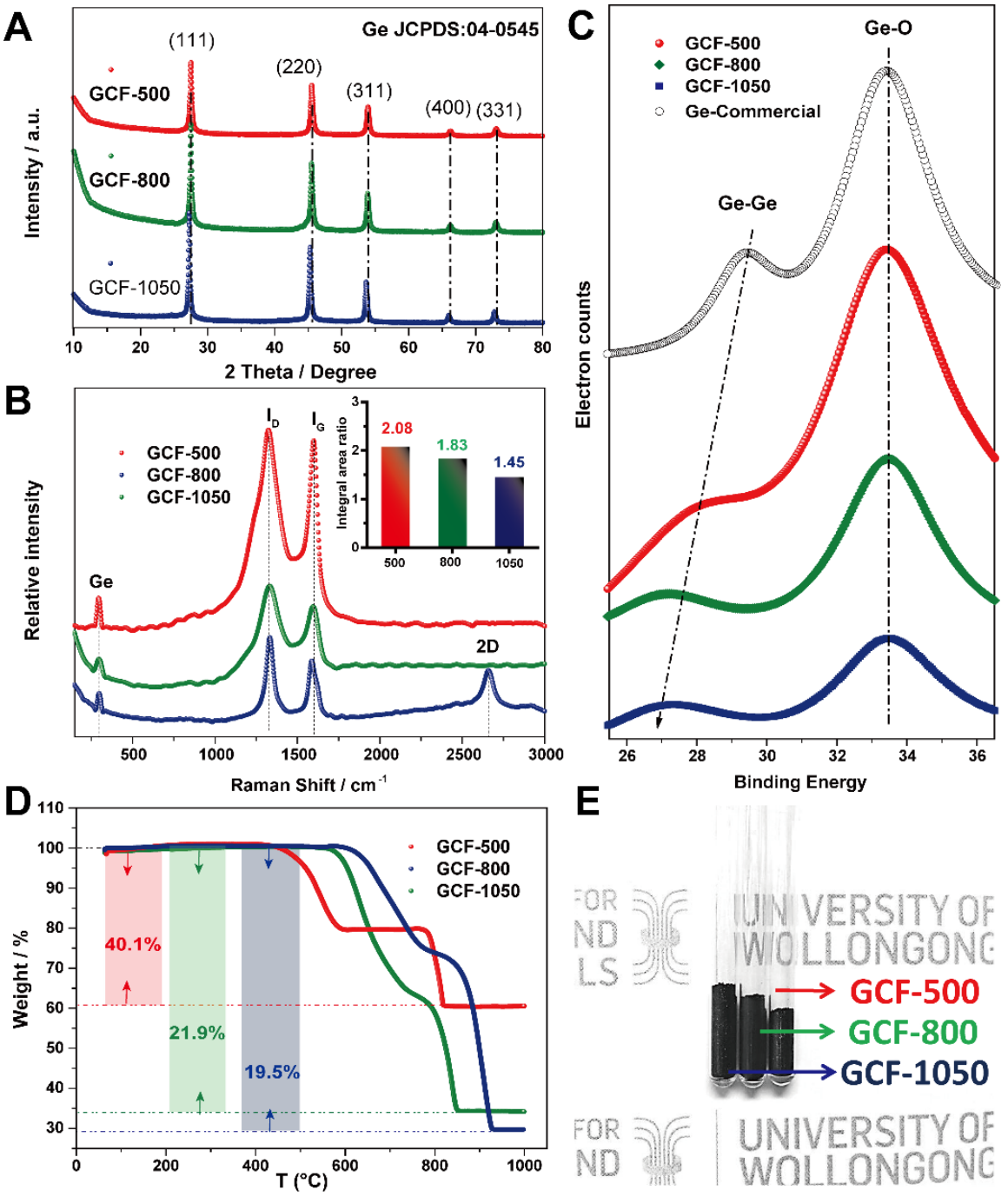

Figure 2 Characterization of the series of GCF materials. (A) XRD curves; a.u.: arbitrary units. **(B) Raman spectra.** The peaks at 299 cm^{-1} correspond to the GeNPs. The sharp peaks at 1332 cm^{-1} and 1590 cm^{-1} can be assigned to the D and G bands of carbon, respectively, [15] while the peak located at ~2650 cm^{-1} in GCF-1050 is assigned to the two-dimensional (2D) band caused by second-order zone boundary phonons. **Inset:** the integral area ratios of the D band to the G band. **(C) XPS spectra of the Ge 3d peaks.** The peak located at 33.5 eV refers

to the Ge-O bonding energy in partial oxidation of Ge surface, while the gradually decreasing binding energy of Ge-Ge bonds indicates a difference in the surface electronic state.[16] **(D) TGA data**. Assuming complete combustion of the carbon layer and conversion from Ge to GeO_2. GCF-500 shows a weight loss from about 400 °C that continues up to 600 °C, indicating the decomposition of amorphous carbon. The following visible weight loss platform observed from 620 °C to 800 °C is mainly attributed to the decay rate balance between Ge oxidation and carbon combustion. After that, the third stage weight loss that starts above 800 °C and finishes at ~ 850 °C can be ascribed to the reaction of residual graphitic carbon. The slightly higher decomposition temperature in TGA curves for GCF-800 (around 550°C) and GCF-1050 (around 620°C) is possibly due to the higher content of graphitic carbon, which is more temperature-resistant than amorphous carbon. **(E) Tap densities.** Each vial contains 0.1 g of tightly packed powders.

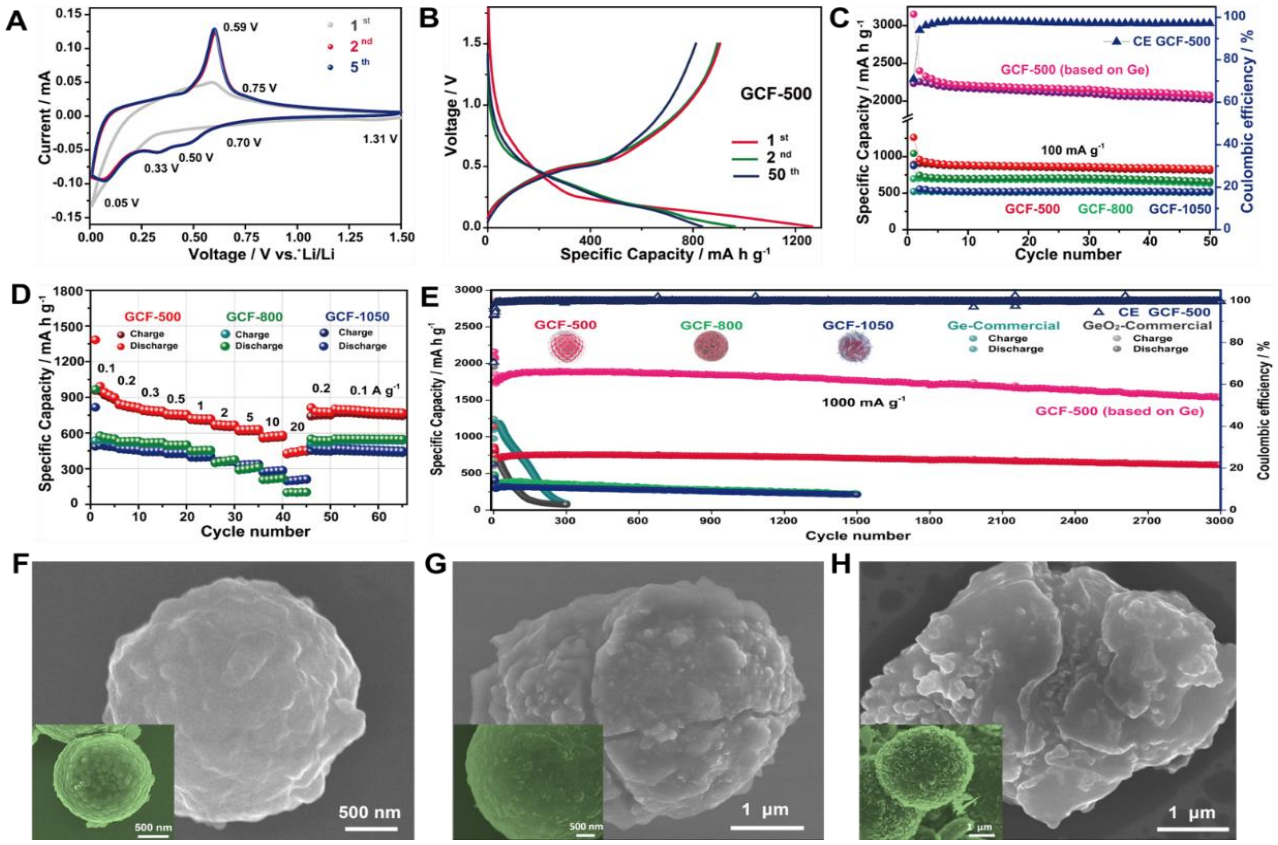

Figure 3 Electrochemical characterization of GCF anodes. (A) Cyclic voltammetry (CV) profiles of GCF-500 corresponding to the selected cycles at a scan rate of 0.1 mV S^{-1}. **(B)** Voltage-capacity profiles for the GCF-500 plotted for the 1st, 2nd, and 50th cycles at a current density of 100 mA g^{-1}. **(C)** Electrochemical cycling performance acquired under a current density of 100 mA g^{-1}. The coulombic efficiency is only plotted for GCF-500. **(D)** Rate capabilities of GCF-500, GCF-800, and GCF-1050 anodes. **(E)** Cycling stability over ultra-long 3 000 galvanostatic cycles of the GCF-500 anode. GCF-800, GCF-1050, commercial Ge, and commercial GeO_2 are also tested under identical conditions. The coulombic efficiency is collected here for GCF-500 only. The rate was activated under 200 mA g^{-1} for the first ten cycles and conducted at 1 000 mA g^{-1} for the later thousands of cycles. Typical **SEM images** of the proposed structures after 200 cycles: **(F)** GCF-500, **(G)** GCF-800, and **(H)** GCF-1050. **Inset images:** the typical structures acquired before cycling.

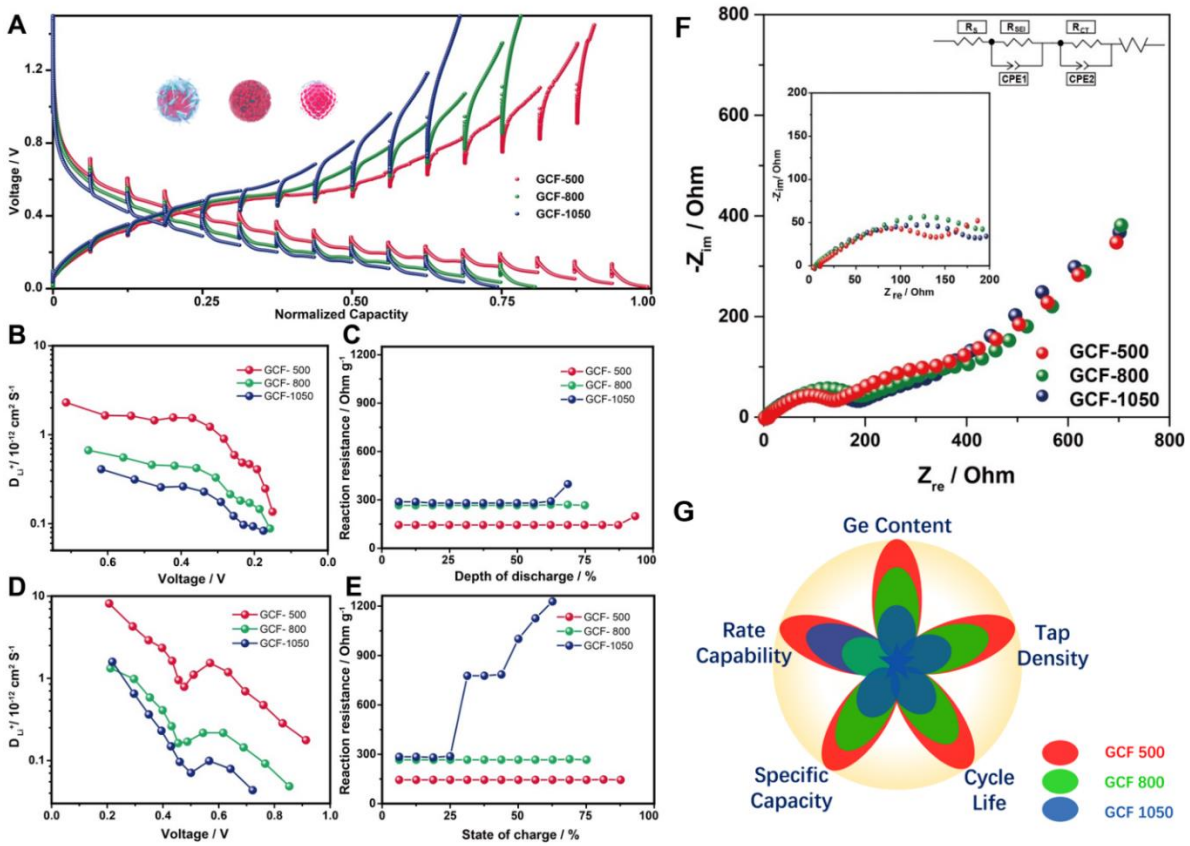

Figure 4 Electrochemical kinetic analysis of lithium storage behaviour of GCF anodes. GITT measurements were conducted between 0.01 V and 1.5 V vs. lithium to determine the diffusion coefficient and reaction resistance parameters. The reaction resistances during charge and discharge processes are obtained by evaluating the overpotential values, defined as the voltage drop between the end of the relaxation step and the start of the pulse step. **(A)** Potential response curves with normalized specific capacity. The normalized capacity is based on the 3rd cycle discharge capacity of GCF-500. **(B)** and **(C)** Li^+ ion diffusion coefficients and reaction resistances calculated from the GITT potential profiles as a function of depth of discharge (DOD). **(D)** Li^+ ion diffusion coefficients and **(E)** reaction resistances as a function of state of charge (SOC). **(F)** Nyquist plots of different electrodes at open circuit voltage. **Inset curve**: magnification plots in the range from 0 to 200 Ohm, with the lower left inset showing an enlargement of the high-frequency region. The upper right inset is the fitted circuit diagram. **(G)** Comparison of GCF electrodes with critical parameters.

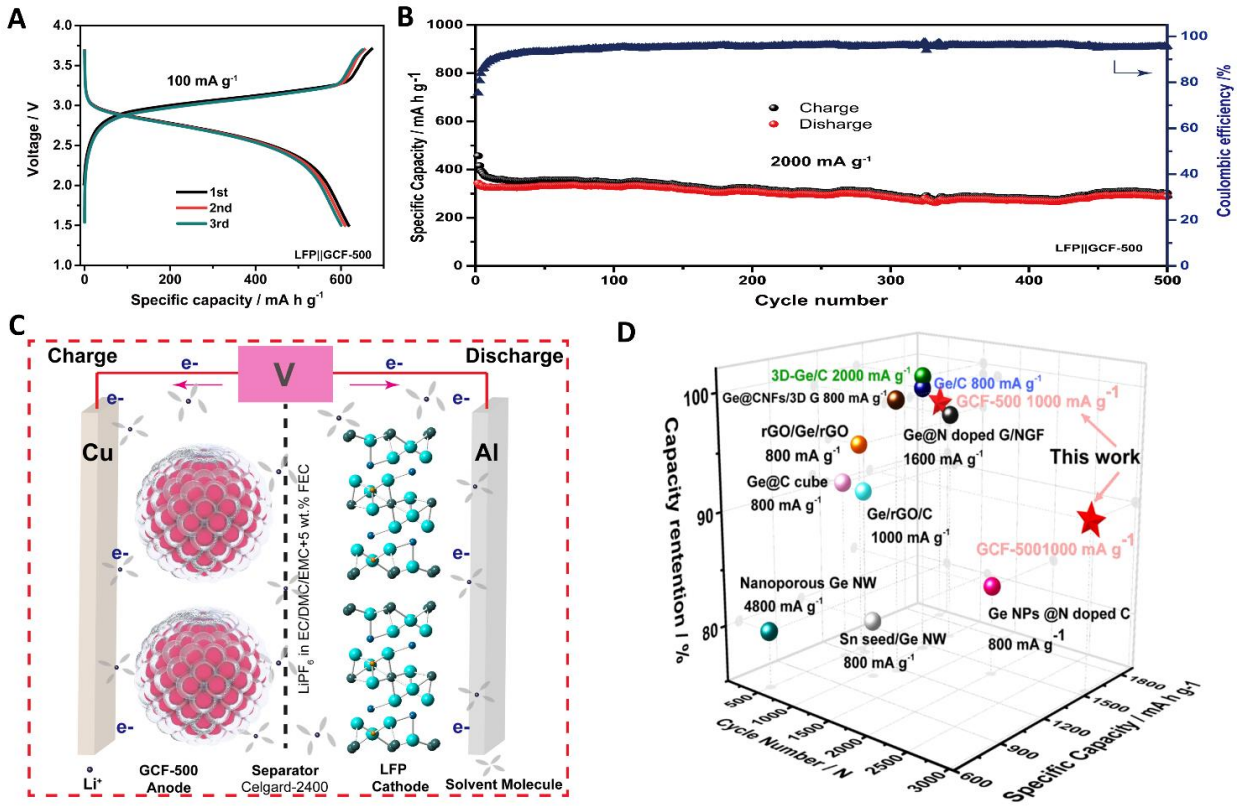

Figure 5 Full cell performance of GCF-500. Lithium-ion full-cell electrochemical performance of GCF-500. **(A)** Charge-discharge curves for the first 3 cycles of the full cell under the current density of 100 mA g^{-1}. **(B)** Long-term cycling performance at 2000 mA g^{-1} for the full-cell. The cell capacity was calculated based on the weight of anode material only. This outstanding performance of the full-cell indicates that LFP‖GCF-500 can serve as a promising cell for practical application. **(C)** Schematic illustration of $LiFePO_4$‖GCF-500 full-cell configuration. **(D)** Comparisons of recent reported Ge materials in lithium-ion batteries, the specific capacities were based on Table S2. The red stars indicate the excellent electrochemical performance of the synthesised GCF-500, not only for the first 1000 cycles but also for 3000 continuous cycles.

Keywords: structural engineering, micro-nanostructures, germanium-carbon frameworks, mechanism understanding, lithium storage

S. Zhang, Y. Zheng, J. Hong, B. Cao, J. N. Hao, Q. N. Fan, T. F. Zhou*, Z. Guo*

Structural Engineering of Hierarchical Micro-nanostructured Ge-C Framework by Controlling the Nucleation for Ultralong-life Li Storage

TOC

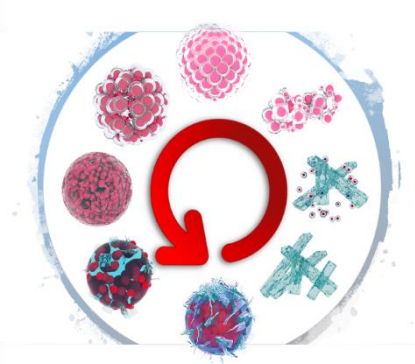

A multi-functional hierarchical micro-nanostructured Ge-C framework is successfully obtained through a scalable structural engineering protocol by controlling the nucleation of metal-organic precursor. The unique micro-nanostructured can effectively inherit the advantages of both microsized and nanosized structures, thus tackling most of the issues involved in Ge-anodes with inferior electrochemical performance under higher current density in half / full cells.